

Dynamical behavior of a complex fluid near an out-of-equilibrium transition: approaching simple rheological chaos

Jean-Baptiste Salmon, Annie Colin, and Didier Roux

Centre de Recherche Paul Pascal, Avenue Schweitzer, 33600 PESSAC, FRANCE

(Dated: March 22, 2002)

We report here an extensive study of sustained oscillations of the viscosity of a complex fluid near an out-of-equilibrium transition. Using well defined protocols, we perform rheological measurements of the onion texture near a layering transition in a Couette flow. This complex fluid exhibits sustained oscillations of the viscosity, on a large time scale (500 s) at controlled stress. These oscillations are directly correlated to an oscillating microstructural change of the texture of the fluid. We observe a great diversity of dynamical behavior and we show that there is a coupling with spatial effects in the ∇v direction. This is in agreement with a careful analysis of the temporal series of the viscosity with the dynamical system theory. This analysis indicates that the observed dynamical responses do not strictly correspond to 3-dimensional chaotic states, probably because some spatio-temporal effects are present and are likely to play an important role.

PACS numbers: 83.10.Gr, 47.50.+d, 83.85.Cg

I. INTRODUCTION

Foams, pastes, liquid crystals, polymers or emulsions share all a common property : when submitted to a shear flow, they exhibit different unusual behavior. They are known as *complex fluids*. Rheological properties of these types of materials have been extensively studied mainly because they exhibit non-Newtonian behavior. If in terms of mechanical behavior, these systems have been relatively well described, the question of the microscopic origin of these effects has only been addressed more recently. Indeed, all complex fluids are composed of a macromolecular architecture which leads to a coupling between their structures and the flow. In the 80's the development of techniques allowing to measure the structure of the fluids under shear allowed the community of physicists to have in parallel informations on the rheological behavior and on the microstructure under flow [1, 2, 3]. One of the questions addressed by this type of approach is related to the very nature of the coupling between structure and flow; indeed this coupling may modify the structure of the fluid undergoing shear flow. It is now quite clear that a pure mechanical approach is not enough to understand the experimental behavior [4, 5]. Recently, a lot of different experimental systems have shown that shear can be coupled to a thermodynamical phase transition [6, 7, 8] but new types of organisation may appear under shear which are not existing at rest [3, 9, 10]. Theoretical approaches tried to describe this complex behavior as a coupling between hydrodynamics and thermodynamics. Even though some success in this way can be noticed [12, 13, 14, 15, 16, 17] we are far from having a satisfying description of the steady behavior of these systems under shear.

Besides the understanding of the structure under steady shear and because these systems exhibit out-of-equilibrium transitions we do expect an even richer behavior. Indeed, it has been shown experimentally, that near out-of-equilibrium transitions, the temporal behavior of the viscosity of a complex fluid, namely lyotropic systems, may exhibit sustained oscillations [18, 19, 20, 21, 22, 23]. The origin of the latter is still unknown, but some authors suggest different scenarios : coupling with shear induced structures [19], mechanical instability in a shear banding case [21] or coupling with elastic instabilities [18]. It has been also suggested that the rheology of wormlike micelles can exhibit chaotic behavior [21]. Theoretically, with a microscopic model some authors found *rheo-chaos* in the rheology of a nematic liquid crystal [24]. Other authors proposed theoretical models [25], based on the equations of the rheology of soft glassy materials [12], in which sustained oscillations of the shear rate at an imposed stress take place. Very recently, the same authors have found *rheo-chaos* in such spatially homogenous models [26]. The aim of this paper is to make an extensive study of an experimental system where sustained oscillations have been previously observed [19]. In the system studied here, a close-compact assembly of soft elastic spheres (onions) [27, 28], it has been early assessed [29] that the theory of bifurcations may be a guide for the understanding of the temporal rheological behavior of the complex fluid. This article presents new experimental results concerning the great diversity of temporal observed responses near an out-of-equilibrium transition. In a first step we carefully study using several protocols the temporal behavior of the rheological signals. We try to evidence a dynamical scenario which may indicate the presence of an Hopf bifurcation. In a second part we relate this rheological behavior to the structural evolution of the fluid using light scattering. The last part of the work is related to a careful analysis of the complex temporal behavior we get in certain cases (resembling to chaos). We show with the help of dynamical system theory that the oscillating viscosity may not simply be described with a 3-dimensional dynamical system, probably because spatio-temporal effects are

playing an important role.

II. DYNAMICAL BEHAVIOR OF THE RHEOLOGY OF THE ONION TEXTURE

The complex fluid we consider here is a lyotropic lamellar phase prepared with SDS (6.5 %wt), octanol (7.8 %wt) and water salted with 20 g.l⁻¹ of sodium chloride. At equilibrium, this phase is made of membranes (surfactant bilayers) of thickness $\delta = 2$ nm, regularly stacked and separated by solvent. The distance between the lamellae, the smectic period d , measured with neutron scattering, is about 15 nm [30]. Such a system is stabilized by entropic interactions due to exclusion between the undulating membranes [31]. This system is sensitive to temperature : at 34°C, a diphasic sponge-lamellar mixture appears [32, 33].

To probe the rheological properties of this complex fluid, we use the experimental device presented in Fig. 1.

In order to measure the viscosity, the lamellar phase is confined in Mooney-Couette cells with gap $e = 1$ mm or $e = 0.5$ mm, height $h = 30$ mm and inner radius $R = 24$ mm. A stress controlled rheometer (AR1000 TA Instrument) allows us to impose a torque on the axis, on which the rotor is fixed, and so to induce a controlled stress σ in the fluid. The rheometer records continuously the shear rate $\dot{\gamma}$ as a function of time, the time scale of this measurement is very short compared to the time scales of the experiment. In order to follow the effect of shear on the microstructure of the phase, the cell is totally transparent and two lasers (He-Ne 15mW) give the diffraction patterns at different heights in the cell. The patterns are collected on a screen and digitalized with a CCD camera (Cohu). Since the laser beams go through the sample twice, one obtains two diffraction rings. The diffraction pattern corresponding to the first sample has an ellipsoidal shape due to the optical deformation of the Couette cell (playing the role of a cylindrical lens). The second sample leads to a classical circular ring. Temperature T is controlled within $\pm 0.1^\circ\text{C}$ using a water circulation around the cell (the range of variation of the latter is about $\pm 0.04^\circ\text{C}$). The experimental behavior observed here, depends strongly on the sample, namely on the concentration of octanol. With a classical setup, we observed that after a few hours (2-3 hours), we have a significant change in the composition due to the evaporation of octanol and water. To control the evaporation of octanol and water and their condensation on the top of the cell, the latter is closed with a thermostated plate, which allows up to 80-hours experiments with the same sample and a negligible evaporation.

The effect of shear on this system has been extensively studied previously [27, 28]. It has been shown that shear controls the texture of the lamellar phase and series of textural transitions are observed as $\dot{\gamma}$ is increased. Small angle light scattering allows us to characterize the different textures which can be obtained at different stress. At low shear rates, a state of partially oriented lamellar phase is observed; at a typical shear rate of 1 s⁻¹, the texture changes radically : the membranes are wrapped in multilamellar vesicles (called onions), close compact organized. The size of these onions is of the order of microns, and scales with shear rate according to $R \sim \dot{\gamma}^{-\frac{1}{2}}$. The diffraction pattern is an homogeneous ring (cf. Fig. 2(a)), indicating that there is no long range correlations between onions.

At $\dot{\gamma} \approx 15$ s⁻¹, six fuzzy peaks appear on the ring (cf. Fig. 2(b)). This corresponds to the *layering* transition [27, 34] : the onions exhibit now a long-range orientational order under shear (which is conserved and evolved into a long-range positional order when the shear is stopped) [27, 28]. In this regime, two dimensional layers of onions with hexagonal order, slide on each other. This transition is named the layering transition after a similar disorder/order transition was observed in colloids under shear [35]. When the shear rate is increased, the peaks on the ring become more contrasted as shown in Fig. 2(c). It is impossible to assess whether the diffraction pattern shown in Fig. 2(b) corresponds to a coexistence between the two different textures or to weak spatial correlations. The spots with wave vectors along the rheometer axis are less intense than the others, this is due to the zig-zag motion of the plans of onions when sliding on each other [35].

Actually the layering transition exhibits different rheological behavior when temperature is changed. When $T \leq 27^\circ\text{C}$, the rheological flow curves σ vs $\dot{\gamma}$ are continuous. It is always possible to define an asymptotic stationary value for the measured shear rate. A typical flow curve σ vs $\dot{\gamma}$, for $T = 26^\circ\text{C}$ and $e = 1$ mm is shown in Fig. 3,

each point corresponds to a stationary state of the shear rate. The different regions A, B and C shown in the flow curve correspond to the different diffraction patterns respectively shown in Fig. 2(a), (b) and (c). In Fig. 4 are shown the temporal responses of the shear rate for the range 14 \rightarrow 17.5 Pa and increment of stress of 0.5 Pa. The temporal behavior of the shear rate become noisier as the critical stress $\sigma_c \approx 16$ Pa is approached. The Fourier transforms of these time series exhibit no peaks so there is no characteristic time in the recorded noisy shear rate.

When $T \geq 27^\circ\text{C}$ and stress is imposed, there is a region where it is difficult to define a stationary viscosity. Typical shear rate responses, on a fresh sample, at an imposed stress near the critical stress σ_c of the layering transition and at a temperature $T = 31^\circ\text{C}$ are shown in Fig. 5; the stationary disordered onion texture appears after about 30 minutes as seen with light scattering. In Fig 5(a), after 10000 s, the recorded shear rate exhibits transitory oscillations with a period of about 500 s, this oscillating regime disappears after 6/7 hours and an *asymptotic stationary* state is reached after 25000 s : the nonlinear rheology of this system exhibits very long time of asymptotisation near the out-of-

equilibrium transition. The second recorded behavior reproduced in Fig. 5(b) has been obtained with the same stress. The asymptotic state for the shear rate differs from the first experiment, this state corresponds to a noisy complex dynamical response : no stationary shear rate can be easily defined. This illustrates the strong dependence on initial conditions for the onset of the temporal instabilities.

The region of dynamical behavior of the viscosity seems to vanish when T approaches 27°C . A convenient way to represent all these effects is to use a *shear diagram*, where *stationary* textures are plotted as a function of T and $\dot{\gamma}$. Such a diagram is plotted in Fig. 6.

As suggested in a precedent work [19], in the region of parameters where dynamical responses occur, the rheological behavior represented by the flow curve must be associated with the temporal responses of the shear rate. In order to show the different *asymptotic* dynamical responses of the shear rate in the vicinity of the layering transition, we must define a protocol in order to get enough reproducibility in the flow curves σ vs $\dot{\gamma}$. Two parameters are important : the stress increment $\delta\sigma$ between two different imposed stress, and the time interval δt we wait before changing the applied stress. If $\delta t \leq 1000$ s the different flow curves are not reproducible and depend drastically on the initial conditions. If $\delta\sigma \geq 1$ Pa we may miss the dynamical region because of its narrowness. Protocols with large δt and small $\delta\sigma$ will correspond to *quasi-static* approaches of the transition. Actually, compromises have been found to use the most quasi-static approach. We are limited by the evaporation of the sample which gives us a maximum of the accessible experimental time (about 80 hours).

For a systematic study we decided to use two different protocols to test the quality of the quasi-static approach we have. We have also used different geometries to try to separate temporal dependence instabilities from spatial structures (cf. Sec. III). For that we made several Couette cells corresponding to different heights and different gaps. We will mainly discuss here the effect of the gap : two different ones have been studied (1 mm and 0.5 mm). Fig. 7 shows two flow curves for two different protocols, both of them with a gap $e = 1$ mm. In protocol I, $\delta t = 7200$ s and $\delta\sigma = 0.5$ Pa, the stress is first increased from 13 to 19 Pa and then decreased from 19 to 13 Pa. The results of the second protocol (protocol II, $\delta t \approx 15000$ s and $\delta\sigma \approx 0.1$ Pa) will be discussed later. The different values reported in Fig. 7 correspond to the mean values of the asymptotic recorded shear rate, and arrows represent oscillations with great amplitude between the maximum and the minimum value of the oscillating shear rate. Figure 8 shows schematically for more convenience, the different results of these protocols. Continuous lines correspond to asymptotic stable states and dashed lines to metastable states.

The flow curve, with protocol I, exhibits six regions of different temporal responses of $\dot{\gamma}$ displayed in Fig. 9.

On the way up :

- Region 1 ($A \rightarrow B$) : relaxation to a stationary state of disordered onions (Fig. 9(a)).
- Region 2 ($B \rightarrow C$) : this is a branch which is followed on the way up, noise appears with a characteristic period of 500 s and an amplitude of about 1 s^{-1} (Fig. 9(b)). Note that even when we wait a very long time with a different protocol no transition seems to appear to the branch $B \rightarrow G$ (we will see that this is different from the branch $C \rightarrow D$).
- Region 3 (C) : the shear rate begins to oscillate after transient phase with a period of 500 s and an amplitude of about 5 s^{-1} (Fig. 9(c)). At the same time six fuzzy peaks appear on the diffraction ring, indicating the onset of spatial correlation between onions (cf. Fig 2(b)).
- Region 4 ($C \rightarrow D$) : the shear rate shows oscillations with a large amplitude of 15 s^{-1} (this corresponds roughly to the distance between the branches $C \rightarrow D$ and $G \rightarrow E$) and with a period of about 500 s (Fig. 9(d)). In this regime the diffraction pattern clearly shows a temporal correlation between the structure of the sample and these oscillations. Modulation of the scattering pattern is observed on the time scale of the rheological signal. When we wait enough time we end up going to the branch $G \rightarrow E$ which is the one followed the way down.
- Region 5 ($E \rightarrow F$) : the shear rate relaxes on a noisy stationary branch (Fig. 9(e)). The corresponding texture corresponds to the diffraction pattern shown in Fig 2(c).

On the way down :

- Region 6 ($E \rightarrow B$) : a complex dynamical state appears progressively. The main period is 300 s and the greatest amplitude is about 5 s^{-1} (Fig. 9(f)). This complex dynamics disappears also when approaching B.

We will come back on the problem of analysing the signal in the last part of this article. Note however than on the way down the branch followed is different from the one followed on the way up. Protocol I allows to record transitory behavior which reveal hysteresis loop and oscillating viscosity. As predicted by the dynamical system theory, one can expect richer dynamical behavior when asymptotic states are reached in the vicinity of hysteresis and oscillating bifurcations [36, 37]. We have seen that transient phases longer than $\delta t = 7200$ s may occur with this system. So in

order to get a better understanding, the experiments were repeated with $\delta t \approx 15000$ s and $\delta \sigma \approx 0.1$ Pa (protocol II on Fig. 7). In this protocol, stress is imposed from B to C. At the point C, a slow drift of shear rate into the region 6 to the point G takes place. Then the stress is imposed from G to A. With the protocol II, region 4 does not exist, the way followed is region 2 \rightarrow region 3 \rightarrow region 6. The large oscillations of region 4 observed in protocol I correspond to metastable dynamics (i.e they do not exist if we wait enough time). This protocol allows to record asymptotic states of the oscillating viscosity : in the vicinity of the point C (region 3), aperiodic oscillations of the shear rate are recorded with a period of 500 s and an amplitude of 3 s^{-1} (Fig. 10).

This aperiodic time serie corresponds to oscillations between a fixed minimum value ($\approx 12 \text{ s}^{-1}$) and a non-fixed maximum value. The region of existence of the latter is very thin, about 0.05 Pa and the transient phases take about 5 hours, so up to 80 oscillations have been recorded before the slow drift ($C \rightarrow G$) of the shear rate into the region of complex dynamics (region 6) takes place. The dynamics in region 6 shown in Fig. 11 corresponds to a complex dynamical state, with a period of about 300 s. When stress goes down approaching point B, the quasi-static protocol II allows to show the simplification shown in Fig. 12 of the complex dynamics of region 6. To the precision of the protocol ($\delta t \approx 15000$ s and $\delta \sigma \approx 0.1$ Pa), no simpler dynamics has been recorded. The main difference between the two protocols (i.e. the disparition of region 4) is a well known characteristic of hysteretic behavior : the hysteresis loop is larger ($B \rightarrow D \rightarrow E \rightarrow B$ in protocol I) with small interval of time δt than for larger δt ($B \rightarrow C \rightarrow G \rightarrow B$ in protocol II) [38]. With the protocol II we can assess that the loop ($B \rightarrow C \rightarrow G \rightarrow B$) corresponds to a real hysteresis loop between region 2 and region 6.

The same rheological measurements were performed with a gap $e = 0.5$ mm, with the protocol I but from 14.5 to 18 Pa then from 18 to 13.5 Pa, the corresponding flow curve is shown in Fig. 13. The flow curves with the gaps $e = 0.5$ and $e = 1$ mm are similar. The confinement does not affect strongly the complexity we observed because all the dynamical scenario (i.e. the six regions in a non-asymptotic protocol) is observed. The hysteresis loop and the different oscillating regimes still exist in the small gap. However some rheological differences must be noticed :

- In a non-asymptotic protocol, as shown in fig. 14, larger oscillations in region 4 ($20 \text{ s}^{-1} \rightarrow 50 \text{ s}^{-1}$) are obtained with $e = 0.5$ mm more easily than with the larger gap ($25 \text{ s}^{-1} \rightarrow 40 \text{ s}^{-1}$). They have also a more relaxational shape than for the larger gap (i.e. the transition from low values to high values is sharper).
- The *hysteresis* cycle ($B \rightarrow D \rightarrow E \rightarrow B$) still exists, but is larger in the confined geometry than for $e = 1$ mm (cf. Figs. 7 and 13, $\dot{\gamma}_0 \approx 15 \text{ s}^{-1}$, $\dot{\gamma}_1 \approx 55 \text{ s}^{-1}$ for $e = 0.5$ mm and $\dot{\gamma}_0 \approx 15 \text{ s}^{-1}$, $\dot{\gamma}_1 \approx 45 \text{ s}^{-1}$ for $e = 1$ mm).
- With the gap $e = 1$ mm, the branch $F \rightarrow G$ does not strictly correspond to the branch $G \rightarrow F$ (cf. Fig. 7).

These effects will be discussed in the next Section. We have seen that a very rich temporal dependence behavior is seen approaching a layering transition. Several protocols have been followed together with different cells. We have shown that it exists a true hysteresis loop which persists when the sampling time of the experiment is increased and which depends on the geometry of the experiment. We have also seen that sustained oscillations can be observed but in a metastable way. A very rich signal can also be obtained which can eventually be seen as chaotic. In what follows we will address first the nature of the temporal dependences. More specifically we want to understand how much these temporal dependences are related to textural changes. Then, we will try to address the question of the nature of the complex signal (whether it is chaotic or not).

III. A COUPLING BETWEEN TEMPORAL INSTABILITIES, STRUCTURE AND SPATIAL INSTABILITIES

We have seen that complex dynamics can be described in this system. A previous work has shown that the observed oscillations of shear rate were correlated to structural changes in this complex fluid system [19] : the fluid oscillates between high shear rate values corresponding to the layered state and low shear rate values corresponding to the disordered state. In fact, there are also macroscopic instabilities that occur in complex fluids : bands in the vorticity direction and in the ∇v direction may appear in the vicinity of out-of-equilibrium transitions (vorticity and shear banding). These instabilities have been extensively studied both theoretically and experimentally [8, 39, 40, 41]. These macroscopic instabilities may lead to a coupling with the dynamical observed behavior in our system. In this Section, we report arguments to show that the vorticity direction is irrelevant for the dynamical recorded shear rate and we suggest that coupling with spatial structures in the ∇v direction may occur.

Observing the sample with naked eyes allows us to see quite a lot of inhomogeneities in the vorticity direction. These inhomogeneities can be described as horizontal bands. These bands have a weak contrast and delimit the Couette cell into different regions of turbidity. There is also no selection of a wavelength, and thus no systematic number or size of bands have been seen. The typical range of observed size is 0.1 mm to 10 mm. These bands appear systematically during transient phases and rarely in asymptotic states. They appear roughly at the level of point B

and persist until point F. The dynamics of these bands seems not correlated to the dynamical recorded viscosity. To understand better the coupling between these macroscopic structures and rheology, we decide to use the diffraction patterns recorded on the CCD (cf. Fig. 1) at two different heights in the cell. The direct beam of the laser is hidden by a beam stop to avoid the saturation of the signal. A contrast parameter ϕ can be defined. It is convenient to define it as naught in the high symmetry texture (disordered state of onion) and different from zero in the low symmetry texture (layered state). We chose to define ϕ as the difference between the mean intensity of scattered light in a region of the ring where a peak appears and the mean intensity on a region of the ring where no peak ever appear (cf. Fig. 2). In a region where no structural changes occur, we checked that ϕ does not depend on the shear rate $\dot{\gamma}$. In fact below point B and above point E, the stationary states correspond respectively to a ring of scattering ($\phi = 0$) and a modulation of scattered light on the ring ($\phi > 0$). Figure 15 shows contrast parameters ϕ , measured at two different heights z_1 and z_2 ($\|z_1 - z_2\| \approx 1$ cm) in the Couette cell and the corresponding oscillating shear rate in region 4. The similarity between the three time series is obvious. The *local* measures of ϕ (only integrated into the ∇v direction) at two different heights, are directly correlated to the *global* measure of the shear rate. This demonstrates that the shear rate oscillations, if coupled with macroscopic spatial structures, are invariant under a z -translation in the Couette cell even though inhomogeneities can be observed. The results shown in Fig. 15 are (i) the existence of correlations between the oscillating viscosity and the microstructure of the phase, (ii) their presence in all the height of the cell. Indeed we tried different Couette cells presenting different heights (30 and 10 mm). No spectacular changes were observed in the temporal dependence of the signal and the observed dynamical scenario is still present. These observations are still comforting us, in the fact that, vorticity is (at first approximation) irrelevant for the dynamical scenario we observe. The change in the gap was by far more spectacular.

In the precedent Section, rheological measurements were performed in two different geometries with different gaps. A confinement in the gap may change the observed dynamics if spatial structures lying in the ∇v direction were oscillating. In fact the flow curves with $e = 0.5$ mm are quite similar to the flow curves with $e = 1$ mm and the mean periods of the recorded oscillations are equivalent, but some rheological differences were noticed above. There is a new difference when correlation with microstructure is done. The large oscillations observed in a non-asymptotic protocol with $e = 0.5$ mm are directly correlated with the contrast parameter, as shown in Fig. 16. The complex fluid oscillates between the two branches (disordered state and layered state) since ϕ oscillates between zero (isotropy of the ring) and a non-zero value (peaks on the ring) : region 4 corresponds to homogeneous relaxational oscillations for the small gap. For the larger geometry ($e = 1$ mm), there is also correlation between structure and flow as shown in Fig. 17. However, the contrast parameter does not oscillate sharply between zero and a non zero value : there is already an anisotropy of the ring in this region. The system oscillates between a state where spatial correlations are weak (low shear rate values) to a state where the latter are strong (high shear rate values). In the larger gap, the region 4 corresponds to oscillations between a mixture of these states. So this may correspond to a separation in different oscillating ordered structures in the ∇v direction. If such spatial structures in the ∇v direction were existing, the flow curves will depend on the gap since spatial effects between oscillating structures may be stronger in the large gap than in the small gap. This may explain the observed difference between $F \rightarrow G$ and $G \rightarrow F$ in the flow curve in Fig. 7. The schematic flow curve presented in Fig. 8 correspond to a homogenous case, well fitted by the real flow curve measured with $e = 0.5$ mm. These observations suggest that the ∇v direction is relevant for the dynamical observed scenario.

To summarize the results of this section, there are arguments to show that the observed dynamical complexity does not depend (at first approximation) on the vorticity direction. It depends more on the ∇v direction. However the strong differences between the two geometries ($e = 1$ mm and $e = 0.5$ mm) are observed only in the metastable region. In particular, to the precision of the device ($\delta t \approx 15000$ s and $\delta \sigma \approx 0.05$ Pa), no simplifications of the dynamics of the viscosity were observed with the small gap. We will come back on these results in the Sec. IV.

IV. ANALYSIS OF THE DYNAMICAL BEHAVIOR OF VISCOSITY WITH DYNAMICAL SYSTEM THEORY

At this stage, we would like to spend some time to analyse the observed experimental behavior, following the out-of-equilibrium theories which have been experimentally and theoretically developed in the last 30 years. In particular the complex signal that we observed on branches ($B \rightarrow D$ and $E \rightarrow B$) could eventually be described with low dimensional dynamical systems as recently suggested on other complex fluids [21]. To assess low dimensional chaotic properties, there exist mainly three techniques based on the properties of low dimensional dynamical systems : (i) to exhibit the *transition to chaos*, (ii) to exhibit the deterministic application which creates a strange attractor, (iii) to compute the metric invariants of a strange attractor [42]. The latter method has been used in the following works [21] in the context of rheology of wormlike micelles, but this method required very long time series to give good estimates of the metric invariants (such time cannot be reached in typical rheological experiments), moreover there

are no theories which can give errors for these invariants [42], and finally this method do not provide the topological properties of a strange attractor. For these reasons, we have followed the two other methods to analyse our data. For that we need to recall some basic principles of dynamical system theory and we will use these principles as a framework to analyse our data.

Dynamical system theory describes the properties of solutions of dynamical systems which are sets of Ordinary Differential Equations (ODE). A dynamical system can be written as

$$\dot{X} = f(X, \mu) \quad (1)$$

where X is a n -dimensional vector which evolves according to (1). μ is a p -dimensional vector of parameters which controls the mathematical form of the function f . The solutions of Eq. (1) can be seen as trajectories in a n -dimensional space called the *phase space*. These trajectories cannot cross each other due to the unicity of solution for a given initial condition. In a lot of physical systems, dissipation of energy occurs, this characterizes a *dissipative* system. In such systems, after a transient phase, all the trajectories collapse on a subspace \mathcal{A} , called the *attractor*. The dimension of this attractor has the following property due to dissipation : $d(\mathcal{A}) < n$. The topological properties of the attractor are of major importance to study the *asymptotic* solutions of a dissipative dynamical system.

Dissipative dynamical systems of dimension 3 may exhibit solutions which are aperiodic [43]. Such solutions are extremely sensitive to initial conditions and their dynamics cannot be predicted. Such solutions are called *chaotic* solutions. In low dimensional dissipative dynamical systems with $n = 3$, which exhibit chaotic solutions, the mathematical condition $2 < d(\mathcal{A}) < 3$ for the dimension of the attractor is required. So such an attractor has *fractal* properties and is called *strange attractor*.

In the theory of dynamical systems, the solution evolves from a stationary state (i.e. $\dot{X} = 0$) to a chaotic state following a set of bifurcations as μ is changed. A bifurcation is the passage from a solution to an other which is not topologically equivalent to the first [44, 45]. The set of bifurcations necessary to create a strange attractor is called the *transition* to chaos. Experimentally, to show such a transition by changing the parameters μ of the experiment is a strong proof for the existence of a chaotic state.

In a lot of physical systems, the presumed model which reproduces the dynamics may have a high number of equations. However when approaching a bifurcation, the *normal form theorem* may allow to reduce the complexity of the equations to a simple equation called the *normal form* which described the dynamics in the vicinity of the bifurcation. Since the bifurcations are not generically simultaneous, the dynamics can be reduced to a low dimensional dynamical system with dimension increasing from 1 as the control parameters are changed. This theorem involves that for complex systems (like rheology of complex fluid), we may expect that the dynamical aperiodic states near an out-of-equilibrium transition, can be expressed as the solutions of a 3-dimensional dynamical system.

In the experiment described above, two parameters μ can be used : the stress σ and the temperature T . Previously different regims of dynamical behavior of the viscosity have been presented. Namely the aperiodic oscillations recorded in the vicinity of the point C (Fig. 10) may be described with a 3-dimensional dynamical chaotic system. As discussed above, if this dynamics corresponds to a chaotic state, a transition to chaos should be present, in particular a Hopf bifurcation leading to a limit stable cycle should exist (i.e. a periodic state). This Hopf bifurcation may lead to the behavior of the Fig. 9(b), where before any transition, the stationary state becomes noisy with a period which is the same as in the aperiodic state. This phenomenon is called *stochastic resonance* and corresponds to the amplification of noise near a Hopf bifurcation [46]. In fact, at the precision of the device ($\delta\sigma \approx 0.01$ Pa, $\delta t \approx 15000$ s and $\delta T = 0.1^\circ\text{C}$) when stress or temperature is varied no periodic asymptotic viscosity has been recorded before this aperiodic state. So if a Hopf bifurcation exists, which is necessary to create a chaotic dynamics, it must be subcritical. Such a case is shown on Fig. 18, where the chosen parameter is stress. When $\sigma < \sigma_1$ the stationary state is stable, there is just stochastic resonance when stress approaches σ_1 (region 2). At stress σ_1 , a stable limit cycle appears with a finite amplitude. Between σ_1 and σ_2 the stable stationary state and the stable limit cycle coexist, but some bifurcations may arise on the cycle which lead to a chaotic dynamics ($N \rightarrow P$). When $\sigma > \sigma_2$ the stationary state is no longer stable and the stable asymptotic state corresponds to a chaotic state. This scenario could eventually correspond to the experimental observed one : region 1 \rightarrow region 2 \rightarrow region 3. In order to assess this hypothesis, when stress oscillates aperiodically at $\sigma \geq \sigma_2$ in region 3, when stress goes down on the branch $P \rightarrow N$, we may expect simplification to a periodic state. To the precision $\delta\sigma \approx 0.01$ Pa and $\delta t \approx 15000$ s, no periodic viscosity has been recorded. This observation means that $\|\sigma_1 - \sigma_2\| \leq 0.01$ Pa. Such an observation has been also checked with temperature as parameter. As discussed above in Sec. III, no simpler dynamics arise when approaching point B when stress goes down from region 6. The only transition we observed is the recorded time serie shown in Fig. 12. So, for the transition $G \rightarrow B \rightarrow A$, no Hopf bifurcation has been seen. However the dynamical responses of the shear rate in the vicinity of point B (Fig. 12) and C (Figs. 5 and 9(b)) strongly suggest the presence of subcritical Hopf bifurcations.

Since no success in showing the scenario related to a Hopf bifurcation has been obtained, one could eventually try to analyse the signal obtained in the aperiodic regime. For that we can use techniques which have been developed to

demonstrate the chaotic nature of experimental data. There are a lot of methods to assess whether a recorded time serie is chaotic of low dimensionality. They involve different invariants : metric, dynamic and topologic [42]. The two first methods compute the metric and dynamic invariants of a strange attractor, such as Lyapunov exponents and various dimensions of the strange attractor. No statistical theory exists that assigns errors to the latter, so it is impossible to determine the validity of the computed invariants. In our case, the time series recorded in region 3 contain up to 80 oscillations, so it is impossible to use those methods. The third method is based on the topological properties of the strange attractor. Currently 100 oscillations are enough to assess chaotic dynamics. Moreover the sampling time interval is 1 s in the recorded time series, which leads to 500 points per cycle : this is enough to use the method. Strange attractors are topological objects with fractal properties, which allow to have the *sensitive to initial conditions* property between two trajectories. To compute a strange attractor using a time serie, one may use the embedding theorem. Such a theorem conjectures that, for a dynamical system like Eq. (1) the attractor \mathcal{A} constructed with the natural variables $\{X_i(t)\}$ is topologically equivalent to the construction of \mathcal{A} with the following variables : $\{X_i(t), X_i(t + \tau), X_i(t + 2\tau), \dots\}$. This is called the *time delay embedding*. The delay time τ is arbitrary but a useful choice must be found to study an experimental time serie. Other embedding variables can be used like : $\{X_i(t), \dot{X}_i(t), \ddot{X}_i(t), \dots\}$ and other combinaisons. The embedding theorem allows when just one variable is measured as in a lot of experimental devices, to reconstruct the attractor \mathcal{A} without knowing all the variables of the dynamical system.

Let us first present a typical case, we will use this case in a modified way at the end of the article. Such a construction is given for the Rössler system, with $(a, b, c) = (0.3, 0.3, 4.5)$:

$$\begin{cases} \dot{x} &= -y - z \\ \dot{y} &= x + ay \\ \dot{z} &= b + z(x - c) \end{cases} \quad (2)$$

Such a system exhibits chaotic solutions for the given parameters. The numerical integration of this system is shown in Fig. 19(a) where the variable $z(t)$ is reproduced. In Fig. 19(b) is shown the embedded corresponding attractor with a delay time $\tau = 20$, which corresponds to $\tau \approx \frac{T_0}{40}$, where T_0 is the mean period of the signal. To show deterministic chaos, one may find the deterministic application which generates the strange attractor. This topological approach is based on the study of the Poincaré section which corresponds to the intersection of the trajectories lying on the attractor \mathcal{A} and a plan. Such a Poincaré section is constructed and plotted in Fig. 19(c). The chosen Poincaré section corresponds to the plan defined by the normal vector $(-1, 0, 1)$ in the frame $[z(t), z(t + \tau), z(t + 2\tau)]$. The Poincaré section is a line and this corresponds to the dissipation of the Rössler system. When X_{k+1} vs X_k are plotted where X_k corresponds to the abscissa on the Poincaré section of the k-intersection of the trajectory with the latter, (shown in Fig. 19(d)), the corresponding curve has a determined shape with a single maximum and a slope which is greater than 1 at the intersection with the bisecting line. This is called the *first return map*. The time serie shown in Fig. 19(a) does not seem to be predicted, but the construction of the attractor \mathcal{A} , the Poincaré section and finally the first return map reveal the deterministic application which is characteristic of deterministic dissipative chaotic dynamical system. The shape of the first return map allows to predict the (k+1)-intersection of the trajectory with the Poincaré section if the k-intersection is known : this is the deterministic property of the equations. However the single humped shape of the first return map, with an average slope greater than one, permits to have the sensitive to initial conditions property between two trajectories.

In the experimental time series recorded, we have followed carefully the same analysis. Preliminary, a high frequency filter has been used to eliminate the noise due to the frequency of the rotation of the Couette cell. This noise has an amplitude of about 0.05 s^{-1} and corresponds to the high frequency of the rotation of the geometry ($10 \ll 500 \text{ s}$). This procedure leads to the time serie presented in Fig. 20(a). The embedded attractor is constructed using the time delay method, with a delay time $\tau = 40 \text{ s}$ (Fig. 20(b)). The constructed attractor is qualitatively similar to the Rössler's one. So the recorded time serie in region 3 is similar to a chaotic variable of a 3-dimensional dynamical system. To assess this property Poincaré section is plotted in Fig. 20(c) and corresponds to the plan with normal vector $(-1, 0, 1)$. However the first return map shown in Fig. 20(d) exhibits no simple shape. Other Poincaré sections and other choices of τ have been investigated, but no simpler shape has been found. We also varied the filter and defined curvilinear abscissa on the Poincaré section in order to reconstruct the first return map, but no deterministic application has been found.

As a conclusion of this work, we cannot assess that the recorded time series of the shear rate correspond to dissipative deterministic chaos of dimensionality 3, even though a great similarity. This might be, because the statistic we study is very poor : up to 40 oscillations have been studied. This might due also, to a low noisy frequency dynamics. The studied dynamics may also correspond to a 4-dimensional chaotic state but in this case the transition to the latter requires the presence of a 3-dimensional strange attractor which has not been observed. However we cannot exclude that this result suggests that the observed dynamics may be more complex. A few coupling effects with space may

occur and so a spatio-temporal dynamics may be recorded as discussed in Sec. III. Such a case does not lead to a simple shape in the first close return map as we will see later. Actually rheology is an experimental tool used for probing the viscosity of materials. However the measure is only global : the recorded shear rate does not correspond to the local shear rate in the gap. The same occurs for the control parameter : a torque is imposed on the axis of the rheometer, but the local stress induced in the fluid is not known. This two phenomena lead to spatial structures like shear banding and vorticity banding in complex fluid as discussed in Sec. III.

In order to illustrate this kind of effects on a 3-dimensional dynamical system, we present here a simple illustration with the help of the Rössler system. In a case where local spatial structures are oscillating, the rheological global measure corresponds to the sum of these local structures. Three integrations of the Rössler system with $(a, b) = (0.3, 0.3)$ and $c = 4.5; 4.4$ and 4.7 have been made. These variables $\{z_1(t), z_2(t), z_3(t)\}$ may correspond to local chaotic oscillating structures. The sum $Z(t)$ of the three different variables $z_1(t)$, $z_2(t)$ and $z_3(t)$, plotted in Fig. 21(a), may correspond to the global measure of rheological experiments. The topological reconstruction of the first return map is the same as presented above and shown in Fig. 21(b), (c) and (d). The constructed attractor has a similar shape as the Rössler's attractor, however no deterministic shape is found for the first return plot. So the dynamical variable $Z(t)$ does not simply corresponds to dissipative deterministic chaos of dimensionality 3. This illustrates that a few spatial effects could lead to the results presented concerning the recorded shear rate. Actually this example is very simple, spatial coupling effects may occur between these three variables, but a more complicated case involving three oscillating variables with non linear coupling terms would provide the same result. In fact the illustration presented here does not prove these structures, it only suggests that a few spatial structures may lead to aperiodic time series which are not strictly chaotic of 3-dimensionality even though the recorded shear rate is qualitatively similar to a 3-dimensional chaotic variable. In fact if more than three local variables were used to reconstruct a global measure, complex dynamical states as presented in Fig. 11 can be reproduced easily. This region does not correspond to simple chaotic dynamic, but this may due to a lot of spatio-temporal effects.

V. CONCLUSION

In this article we have presented a detailed experimental study of the dynamical behavior of the rheology of a complex fluid near a textural instability. We have shown that a complex behavior with different regims as a function of time can be described. Among the most interesting regimes, sustained oscillations and *chaotic like* types of signals have been observed. We have shown that the temporal dependence is related to textural changes involving the whole sample. We spend sometime to analyse the *chaotic like* signal, using a careful mathematical analysis. We cannot prove that the signal corresponds really to a 3-dimensional chaotic system, even though it has several distinctive features resembling to a 3-dimensional deterministic chaotic state. To conclude, to interpret the signal we have, we make the hypothesis that there is a coupling between temporal behavior and spatial instabilities involving a finite but small number of cells. We have also shown with rheophysics tools that such spatial structures are probably in the ∇v direction. A question remains about the microscopic origin of the observed dynamics, it is obviously a complicated problem. However we can make some assumptions according to the experimental results discussed in this Article. First the observed period of oscillations involves long time scales (about 10 minutes), such time scales have been previously observed with the same system in other experiments. Namely it has been shown that the structural response of the onion texture involves time scales of the order of minutes. This behavior was assumed to be related to the displacement of the grain boundaries of the disordered onion texture [11]. In an other context it has been measured with neutron scattering that the smectic period of the ordered onion texture decreases with increasing shear rate [34]. It was assumed that the expelled water was staying between the different layers of the ordered state. When the shear rate is stopped, the swelling kinetics of the compressed onion texture shows strong nonlinear effects on long time scales [28]. Finally, the time scales of reorganization of the onion texture between two different imposed stress are of the order of minutes [47]. The oscillations may be the result of a competition between an ordering of the disordered state driven by the stress (mechanical ordering) and an slow textural evolution which destroys the stress-induced ordered state. These two effects may take place on different time scales and may produce oscillating behavior. Concerning the strong dependence of the observed dynamics with temperature, it may be explained by the dependence on temperature of the time scales discussed above. For example it has been shown that the time scale of the swelling kinetics depend strongly on the temperature, due to the presence of thermally activated defects in the lamellar phase [28].

Acknowledgments

The authors are deeply grateful to Alain Arnéodo for impulsing a lot of ideas in this work. We also thank Sébastien Manneville for fruitful discussions.

-
- [1] N. A. Clark and B. J. Ackerson, Phys. Rev. Lett. **44**, 1008 (1980).
 - [2] C. R. Safinya, E. B. Sirota, R. Plano, and R. F. Bruinsma, J. Phys. Condens. Matter **2**, SA365 (1990).
 - [3] O. Diat, D. Roux, and F. Nallet, J. Phys. II France **3**, 1255 (1993).
 - [4] Applied Sciences Kluwer Academic publishers, ed., *Theoretical challenges in the dynamics of complex fluids* (Tom McLeish Series E, 1997).
 - [5] M. E. Cates and M. R. Evans, eds., *Soft and fragile matter : Non equilibrium dynamics metastability and flow* (Institute of Physics Publishing (Bristol), 2000).
 - [6] O. Diat and D. Roux, Langmuir **11**, 1392 (1995).
 - [7] V. Schmitt, F. Lequeux, A. Pousse, and D. Roux, Langmuir **10**, 955 (1994).
 - [8] J.-F. Berret, G. Porte, and J.-P. Decruppe, Phys. Rev. E **55**, 1668 (1997).
 - [9] C. Pujolle-Robic and L. Noirez, Nature **409**, 167 (2001).
 - [10] P. Panizza, P. Archambault, and D. Roux, J. Phys. II **5**, 303 (1995).
 - [11] P. Panizza, D. Roux, V. Vuillaume, C.Y.D Lu, M. E. Cates, Langmuir **12**, 248 (1996).
 - [12] P. Sollich, F. Lequeux, P. Hebraud, and M. E. Cates, Phys. Rev. E **78**, 2020 (1997).
 - [13] A. Onuki, Phys. Rev. A **35**, 5149 (1987).
 - [14] M. E. Cates and S. T. Milner, Phys. Rev. Lett. **62**, 1856 (1989).
 - [15] A. Ajdari, Phys. Rev. E **58**, 6294 (1998).
 - [16] P. D. Olmsted and P. M. Goldbart, Phys. Rev. A **41**, 4578 (1992).
 - [17] R. F. Bruinsma and C. R. Safinya, Phys. Rev. A **43**, 5377 (1991).
 - [18] P. Fischer, Rheol. Acta **39**, 234 (2000).
 - [19] A.-S. Wunenberger, A. Colin, J. Leng, A. Arnéodo, and D. Roux, Phys. Rev. Lett. **86**, 1374 (2001).
 - [20] G. C. Azkarate, Ph.D. thesis, Université Bordeaux I (2000).
 - [21] R. Bandyopadhyay, G. Basappa, and A. K. Sood, Phys. Rev. Lett. **84**, 2022 (2000).
 - [22] Y. T. Hu, P. Boltenhagen, and D. J. Pine, J. Rheol. **42**, 1185 (1998).
 - [23] C. Meyer, S. Asnacios, C. Bourgaux, and M. Kleman, Mol. Cryst. Liq. Cryst. **332**, 531 (1999).
 - [24] M. Grosso, R. Keunings, S. Crescitelli, and P. L. Maffettone, Phys. Rev. Lett. **86**, 3184 (2001).
 - [25] D. A. Head, A. Ajdari, and M. E. Cates, Phys. Rev. E **64**, 061509 (2001).
 - [26] M. E. Cates, D. A. Head, and A. Ajdari (2002), to be published, preprint cond-mat/0204162.
 - [27] P. Sierro and D. Roux, Phys. Rev. Lett. **78**, 1496 (1997).
 - [28] J. Leng, F. Nallet, and D. Roux, Eur. Phys. J. E. **4**, 77 (2001).
 - [29] D. Roux, F. Nallet, and O. Diat, Europhys. Lett. **24**, 53 (1993).
 - [30] P. Herve, D. Roux, A.-M. Bellocq, F. Nallet, and T. Gulik-Krzywicki, J. Phys. II France **3**, 1255 (1993).
 - [31] W. Helfrich, Z. Naturforsch **33a**, 305 (1978).
 - [32] G. Porte, J. Appell, P. Bassereau, J. Marignan, M. Skouri, I. Billard, and M. Delasanti, Physica A **176**, 168 (1991).
 - [33] D. Roux, C. Coulon, and M. E. Cates, J. Phys. Chem. **96**, 4174 (1992).
 - [34] O. Diat, D. Roux, and F. Nallet, Phys. Rev. E **51**, 3296 (1995).
 - [35] B. J. Ackerson and N. A. Clark, Phys. Rev. A **30**, 906 (1984).
 - [36] P. Richetti, J.-C. Roux, F. Argoul, and A. Arnéodo, J. Chem. Phys. **86**, 3339 (1987).
 - [37] F. Argoul, A. Arnéodo, P. Richetti, and J.-C. Roux, J. Chem. Phys. **86**, 3325 (1987).
 - [38] C. Grand, J. Arrault, and M. E. Cates, J. Phys. II France **7**, 1071 (1997).
 - [39] E. Fischer and P. T. Callaghan, Phys. Rev. E **64**, 011501 (2001).
 - [40] J. L. Goveas and P. D. Olmsted, to be published, preprint cond-mat/0104191.
 - [41] A. Spenley, M. E. Cates, and T. C. B. McLeish, Phys. Rev. Lett. **71**, 939 (1993).
 - [42] R. Gilmore, Rev. Mod. Phys. **70**, 1455 (1998).
 - [43] E. N. Lorenz, J. Atmos. Sci. **20**, 130 (1963).
 - [44] J. Guckenheimer and P. Holmes, *Nonlinear Oscillations, Dynamical Systems, and Bifurcations of Vector Fields* (Springer, Berlin, 1984).
 - [45] J. D. Crawford, Rev. Mod. Phys. **63**, 991 (1991).
 - [46] H. Gang, T. Ditzinger, C. Z. Ning, and H. Haken, Phys. Rev. Lett. **71**, 807 (1993).
 - [47] P. Panizza, A. Colin, C Coulon, D. Roux, Eur. Phys. J. B. **4**, 65 (1996).

Figures

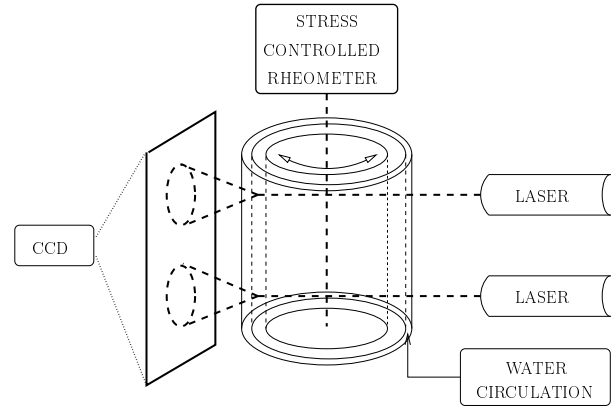


FIG. 1: Experimental setup, a thermostated plate (not shown) on the top of the cell allows to avoid evaporation.

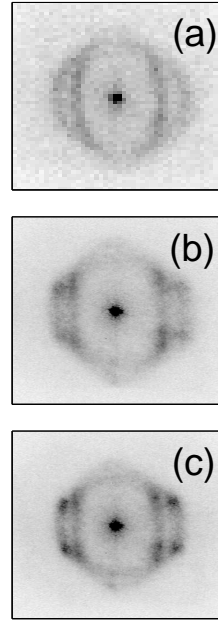


FIG. 2: Diffraction figures obtained under shear. (a) Ring of scattering, (b) Fuzzy hexagonal pattern, (c) Hexagonal pattern.

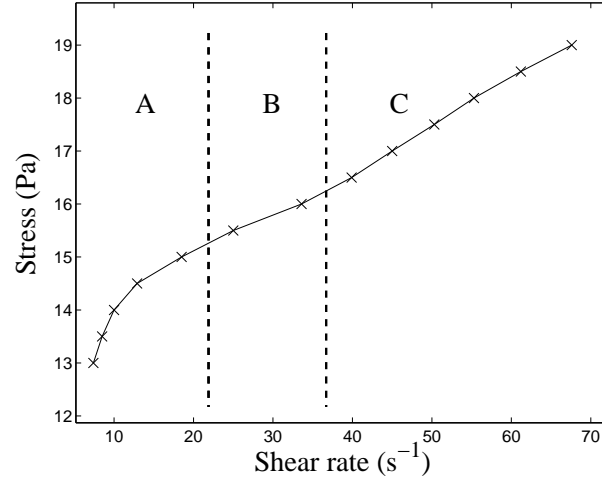


FIG. 3: Flow curve at $T = 26^\circ\text{C}$, $e = 1$ mm. The regions A, B and C correspond to the different diffraction patterns shown in Fig. 2.

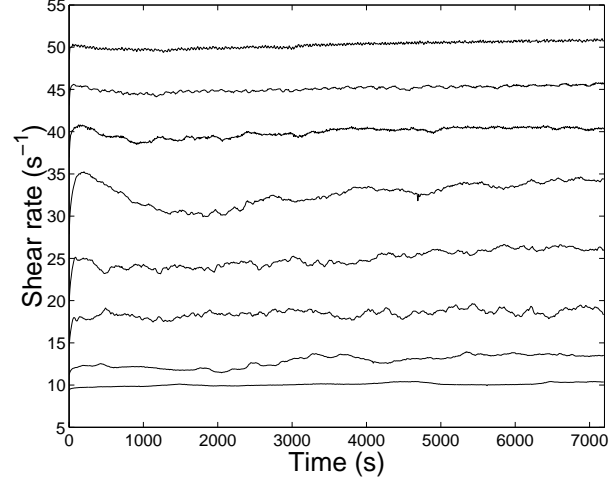


FIG. 4: Temporal responses of the shear rate for the range $14 \rightarrow 17.5$ Pa of imposed stress with increment $\delta\sigma = 0.5$ Pa, corresponding to the flow curve shown in Fig. 3.

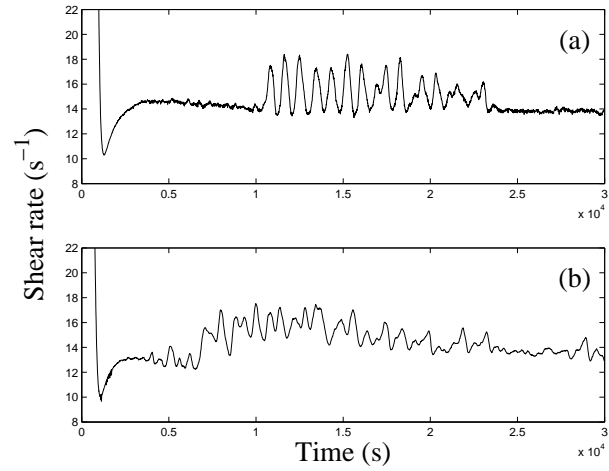


FIG. 5: Typical shear rate responses at an imposed stress ($\sigma = 15$ Pa, $T = 31^\circ\text{C}$) near the layering transition.

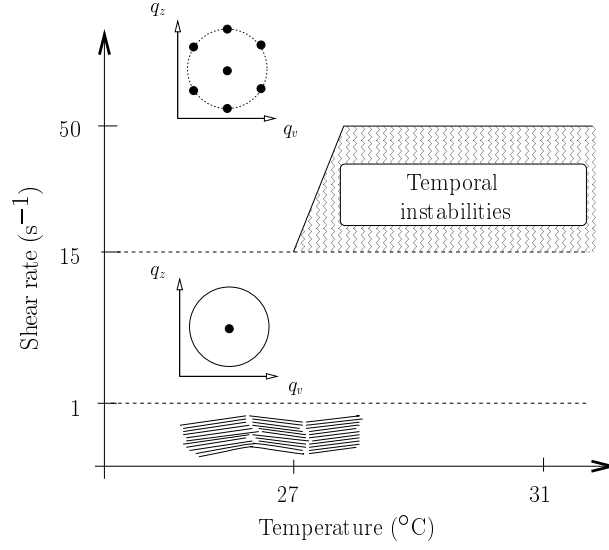


FIG. 6: Shear diagram of the lyotropic lamellar phase studied, the gray region corresponds to non-stationary shear rate responses at stress controlled.

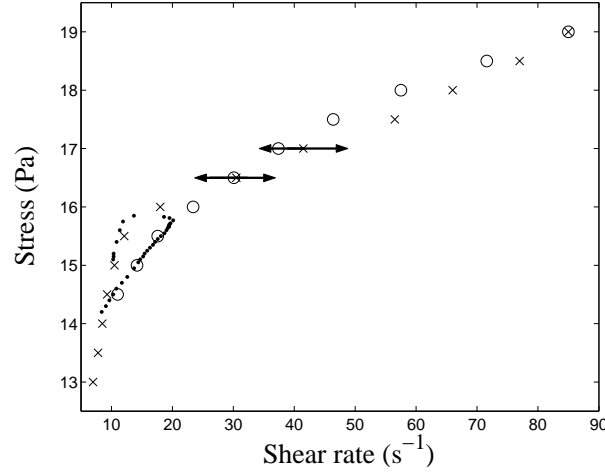


FIG. 7: Different flow curves with $T = 30^\circ\text{C}$ and $e = 1$ mm, for two different experimental procedures. \times correspond to protocol I, stress up. \circ correspond to protocol I, stress down. \cdot correspond to protocol II.

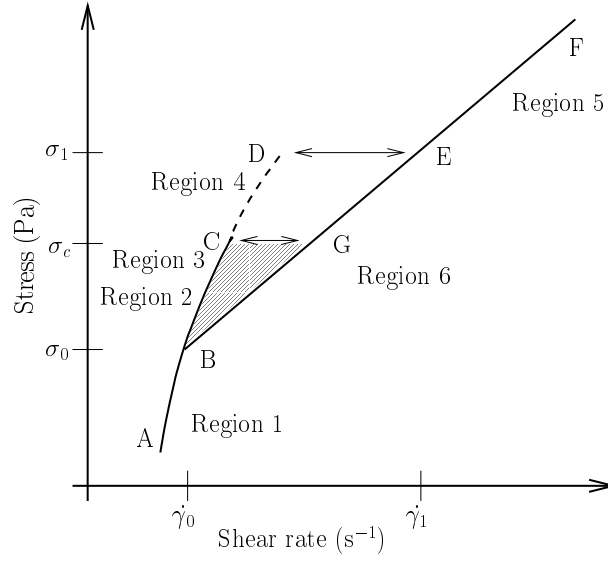


FIG. 8: Schematic representation of the asymptotic states (solid lines), metastable states (dashed line) in the vicinity of the layering transition, and their corresponding dynamical regions.

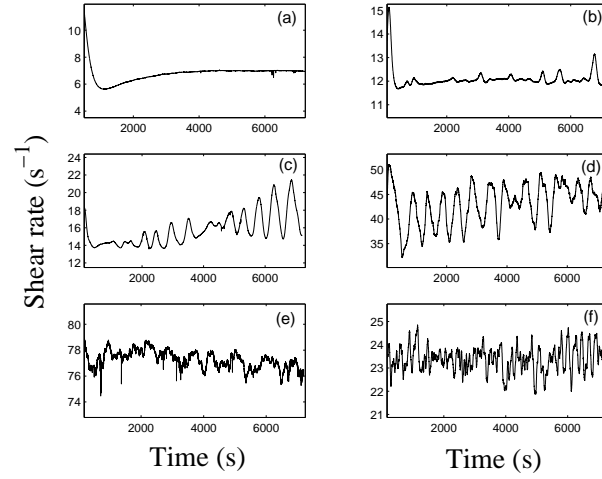


FIG. 9: Different dynamical responses of the shear rate in the vicinity of the layering transition with $e = 1$ mm. Note the different amplitudes of these temporal responses. (a) Region 1 ($\sigma = 13\text{Pa}$), (b) Region 2 ($\sigma = 15.5\text{Pa}$), (c) Region 3 ($\sigma = 16\text{Pa}$), (d) Region 4 ($\sigma = 17\text{Pa}$), (e) Region 5 ($\sigma = 18.5\text{Pa}$), (f) Region 6 ($\sigma = 16\text{Pa}$).

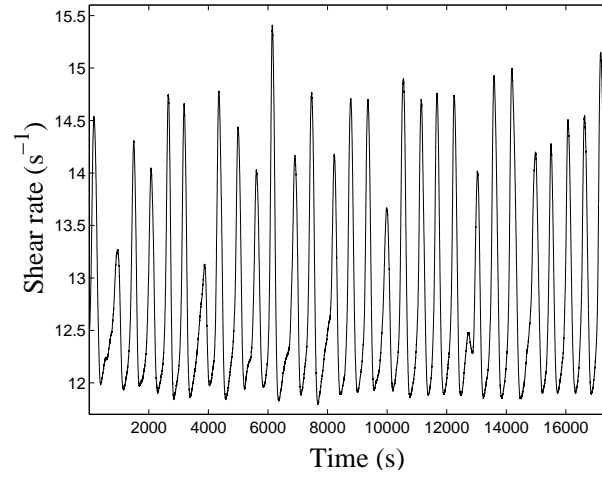


FIG. 10: Aperiodic time serie $\dot{\gamma}(t)$ in region 3.

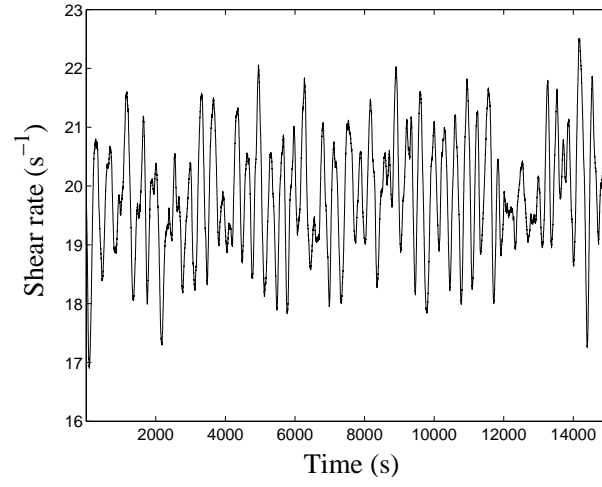


FIG. 11: Complex dynamical time serie $\dot{\gamma}(t)$ in region 6.

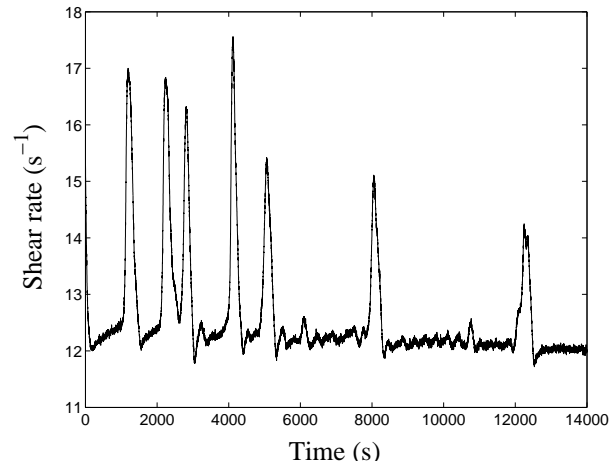


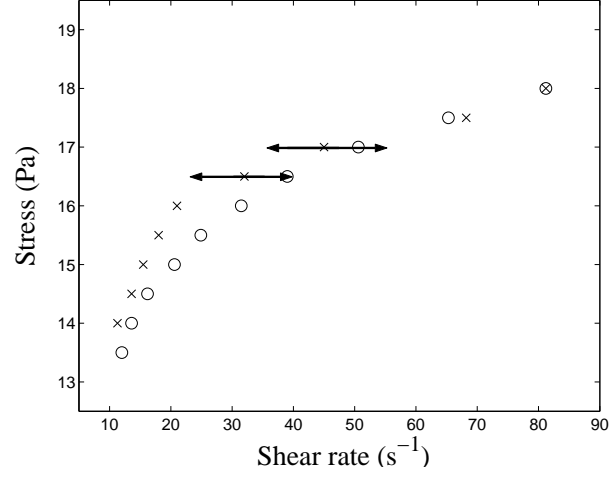
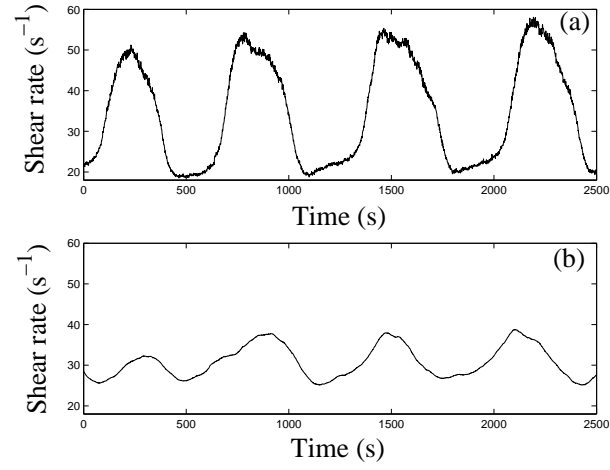
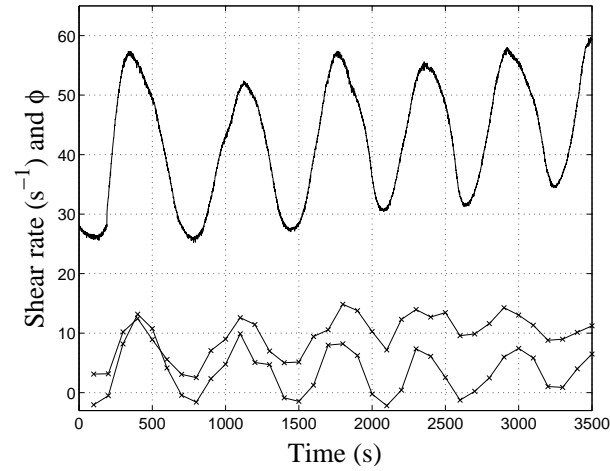
FIG. 12: Typical time serie showing the simplification of the dynamics of region 6 when approaching σ_0 .FIG. 13: Flow curve with $T = 30^\circ C$ and $e = 0.5$ mm for the experimental protocol I. \times correspond to protocol I, stress up. \circ correspond to protocol I, stress down.FIG. 14: Shear rate oscillations in region 4 for two different geometries, (a) $e = 0.5$ mm, (b) $e = 1$ mm.

FIG. 15: Correlation between two contrast parameters ϕ at two different heights in the Couette cell (\times) with a gap $e = 0.5$ mm and $\dot{\gamma}(t)$ (solid line) in region 4.

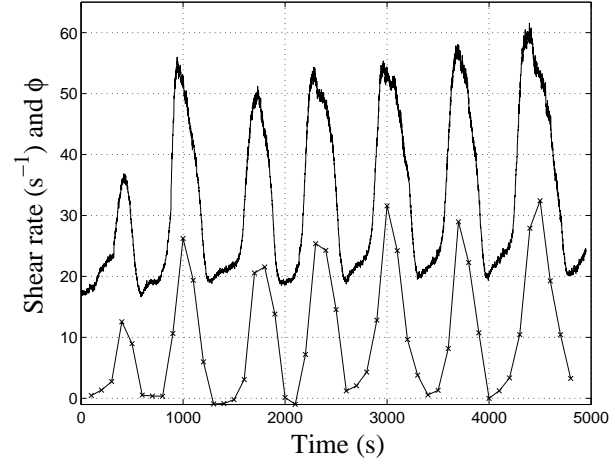


FIG. 16: Correlation between the contrast parameter ϕ (\times) and $\dot{\gamma}(t)$ (solid line) in region 4 with gap $e = 0.5$ mm.

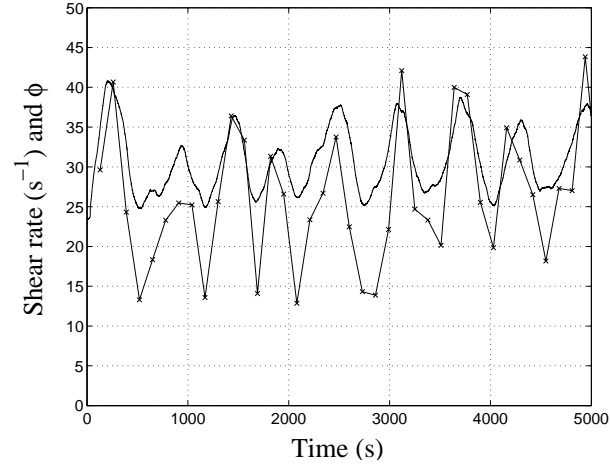


FIG. 17: Correlation between the contrast parameter ϕ (\times) and $\dot{\gamma}(t)$ (solid line) in region 4 with gap $e = 1$ mm.

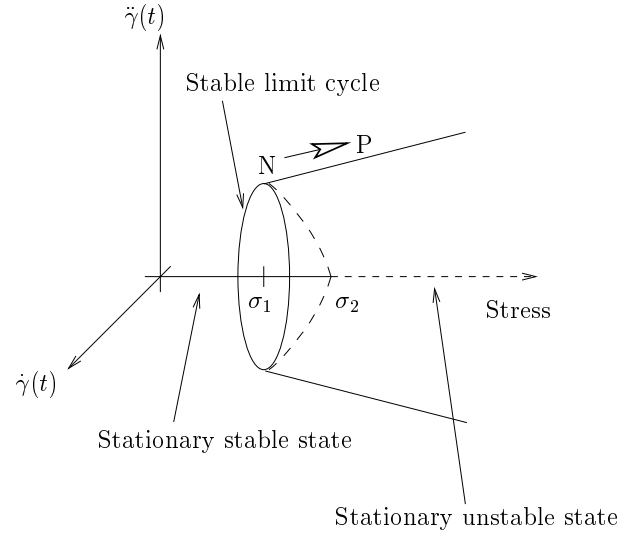


FIG. 18: Subcritical Hopf bifurcation and transition to chaos, σ_2 corresponds to the lost of stability of the stationary state. At stress σ_1 , a limit cycle exists, but between N and P, transition to chaos may occur

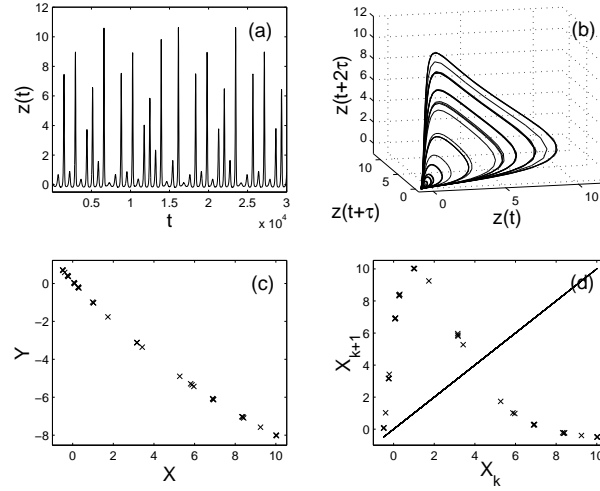


FIG. 19: (a) Solution $z(t)$ of the Rössler system, (b) Embedding reconstruction of the attractor, (c) Poincaré section (d) First return map constructed with the abscissa X of the Poincaré section

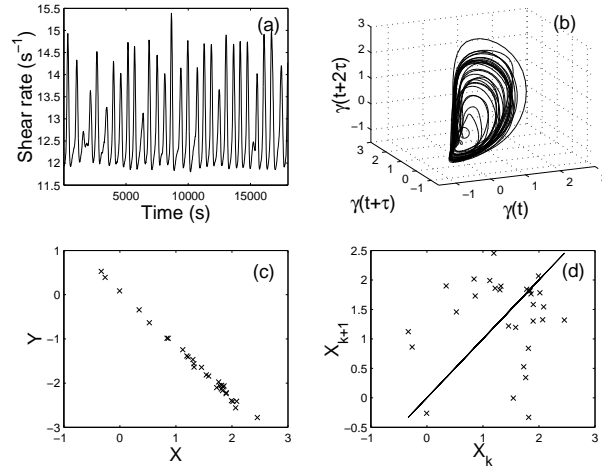


FIG. 20: (a) Analysis of the experimental time series, (b) Embedding reconstruction of the attractor, (c) Poincaré section, (d) First return map constructed with the abscissa X of the Poincaré section

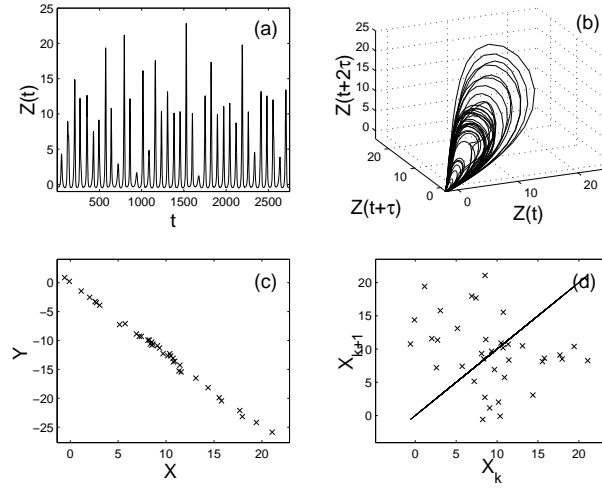


FIG. 21: (a) Analysis of the time series $Z(t)$, (b) Embedding reconstruction of the attractor, (c) Poincaré section, (d) First return map constructed with the abscissa X of the Poincaré section